Journal of Sound and Vibration (2001) **245**(2), 329–345
doi:10.1006/jsvi.2001.3577, available online at http://www.idealibrary.com on IDEAL®

ORTHOGONAL FUNCTION IN MOVING LOADS IDENTIFICATION ON A MULTI-SPAN BRIDGE

X. Q. Zhu and S. S. Law

Civil and Structural Engineering Department, Hong Kong Polytechnic University, Hung Hom, Hong Kong, People's Republic of China. E-mail: cesslaw@polyu.edu.hk

(*Received* 7 *June* 2000, *and in final form* 29 *January* 2001)

Assumed mode shapes are often used to determine the responses of a bridge deck under the passage of moving loads. However, the use of these mode shapes in the inverse problem of force identification would lead to unnecessary errors due to their inherent inaccuracy. Direct differentiation of the measured responses is usually used to obtain the velocities and accelerations, and this practice leads to large errors when measurement noise is included. This paper derives the analytical vibration mode shapes of a continuous beam on rigid supports from the eigenvalue and eigenfunction analysis, thus eliminating the modelling errors from the assumed mode shapes. A generalized orthogonal function approach is proposed to obtain the derivatives of the bridge modal responses, and this eliminates the errors due to measurement noise. The moving loads are identified using the regularization method on the equations of motion. Computational simulations and laboratory test results show that the method is effective and accurate for identifying a group of moving loads.

1. INTRODUCTION

Accurate estimation of dynamic loads acting on a structure is very important for the structural design, control and diagnosis. The indirect load determination is of special interest when the applied loads cannot be measured directly, while the responses can be measured easily. It is an ill-posed inverse problem because the response typically is a continuous vector function in the spatial co-ordinates, and it is defined at a few points of the structure only. Therefore, solutions to the problem are frequently found unstable in the sense that small changes in the responses would result in large changes in the calculated load magnitudes. Lee and Park [1] have analyzed the characteristics of the force determination error in a structural dynamic system, and they proposed a regularization procedure to reduce the error. Tikhonov's regularization method was used by Busby and Trujillo [2] in a modal-based load identification. In a more recent work, Busby and Trujillo [3] used a first order regularization, where the penalty is in terms of the derivative of the force rather than the force itself, and the regularization parameter is determined by the L-curved method [4] and the generalized cross-validation method [5]. Later, a time domain method was presented for estimating the discrete input forces acting on a structure based on the system Markov parameters [6]. The regularization technique was employed to stabilize the computation.

This paper aims at exploring the theory of the moving load identification without knowledge of the load system characteristics in the time domain. O'Connor and Chan [7] modelled a bridge as an assembly of lumped masses interconnected by a massless elastic

0022-460X/01/320329 + 17 $35.00/0

beam element to interpret time-varying moving forces from the equations of motion of the system. Chan *et al.* [8] modelled the bridge as a Euler–Bernoulli beam to form the equations of motion under a set of independent moving forces. Law *et al.* [9] assumed the force to be a step function in a small time interval to relate the bending moment and acceleration of the beam with the time-varying forces, and the equations of motion were solved in the time domain. Later Law *et al.* [10] performed a Fourier transformation on the independent equations of motion of the system that is obtained through modal co-ordinate transformation. Exact solution on the time history of the forces is obtained by performing the inverse Fourier transformation. Zhu and Law [11] investigated the dynamic behavior of a multi-span continuous bridge with a non-uniform cross-section under moving loads using the assumed mode method. The intermediate supports are assumed to have large stiffnesses, and a damped least-squares method was presented to identify the moving loads. The use of assumed mode shapes and the assumption of large stiffness at the intermediate support in the last reference would lead to errors in the identified forces. Lin [12] has mentioned that the selection of support stiffness is problem dependent, and it should be used with care if numerical stability in the solution has to be maintained.

This paper eliminates the modelling error from the assumed mode shapes by using an exact solution on the mode shapes. Rigid intermediate supports are allowed for in a continuous bridge. A generalized orthogonal function approach is proposed to obtain the derivatives of the bridge modal responses from the strain measurements instead of direct differentiation [8, 11]. This would reduce the error due to measurement noise. The accuracy of the identified moving loads on the bridge is improved using the regularization method on the modal co-ordinate equations of motion of the bridge in the time domain. Moving forces on a single-span beam, on a two-span beam, and the axle interaction forces from a four-DOFs vehicle on a triple-span bridge are studied in the simulation. Laboratory study is also conducted on a single-span beam. Computational simulations and laboratory test results show that the method is effective and accurate for identifying a set of moving loads.

2. MOVING LOADS IDENTIFICATION THEORY

2.1. EQUATION OF MOTION

A continuous uniform Euler–Bernoulli beam subjected to a set of moving forces P_l $(l = 1, 2, \ldots, N_p)$ is shown in Figure 1. The forces are assumed to be moving as a group at a prescribed velocity $v(t)$ along the axial direction of the beam from left to right. Assuming the forces as step functions in a small time interval, the equation of motion of the beam can be written as

$$\rho A \frac{\partial^2 w(x,t)}{\partial t^2} + c \frac{\partial w(x,t)}{\partial t} + EI \frac{\partial^4 w(x,t)}{\partial x^4} = \sum_{l=1}^{N_p} P_l(t)\delta(x - \hat{x}_l(t)), \tag{1}$$

where A is the cross-sectional area; E is the Young's modulus, I the moment of inertia of the beam cross-section, c the damping of the beam, $w(x, t)$ the transverse displacement function of the beam, $\hat{x}_l(t)$ the location of moving force $P_l(t)$ at time t, and $\delta(t)$ the Dirac delta function. Express the transverse displacement $w(x, t)$ in modal co-ordinates as

$$w(x,t) = \sum_{i=1}^{\infty} \phi_i(x) q_i(t), \tag{2}$$

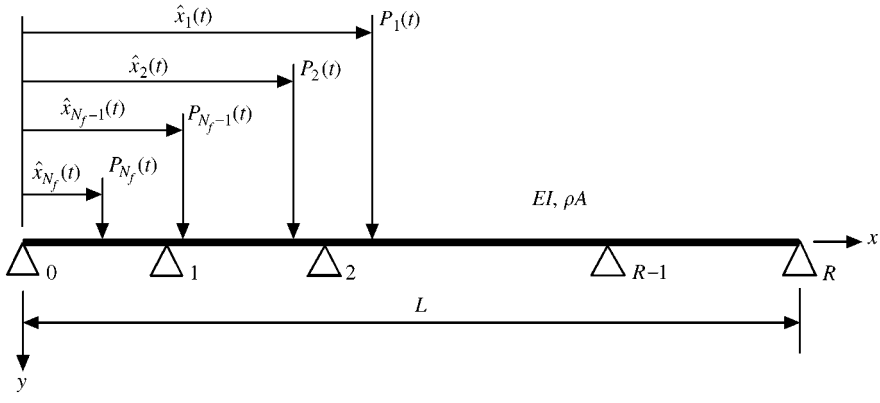

Figure 1. A continuous beam subjected to moving forces.

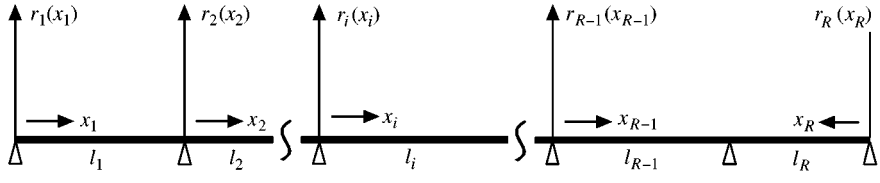

Figure 2. An R-span continuous beam.

where $\phi_i(x)$ is the mode shape function of the ith mode, which is determined from the eigenvalue and eigenfunction analysis proposed by Hayashikawa and Watanabe [13] as shown below; $q_i(t)$ is the ith modal amplitude. Substituting equation (2) into equation (1), and multiplying by $\phi_i(x)$, integrating with respect to x between 0 and L, and applying the orthogonality conditions, we obtain

$$\frac{\mathrm{d}^2 q_i(t)}{\mathrm{d}t^2} + 2\xi_i\omega_i \frac{\mathrm{d}q_i(t)}{\mathrm{d}t} + \omega_i^2 q_i(t) = \frac{1}{M_i} \sum_{l=1}^{N_p} P_l(t)\phi_i(\hat{x}_l(t)), \tag{3}$$

where ω_i, ξ_i, M_i are the modal frequency, the damping ratio and the modal mass of the ith mode, and

$$M_i = \int_0^L \rho A(x)\phi_i^2(x)\,\mathrm{d}x. \tag{4}$$

2.2. EIGENVALUE AND EIGENFUNCTION OF A CONTINUOUS BEAM

The eigenfunction of an R span Euler–Bernoulli continuous beam as shown in Figure 2 can be written in the following form:

$$r_i(x_i) = A_i \sin\beta x_i + B_i \cos\beta x_i + C_i \sinh\beta x_i + D_i \cosh\beta x_i \quad (i = 1, 2, \ldots, R), \tag{5}$$

where $r_i(x_i)$ is the eigenfunction for the ith span, and β is the eigenvalue. Hayashikawa and Watanabe [13] have presented the formulation of the eigenfunction with arbitrary

boundary conditions. The same problem is solved for a multi-span continuous beam by the authors, and the boundary conditions are listed as follows:

$$r_i(x_i)|_{x_i=0} = r_i(x_i)|_{x_i=l_i} = 0, \quad (i = 1, 2, \ldots, R)$$

$$\left.\frac{\partial^2 r_1(x_1)}{\partial x_1^2}\right|_{x_1=0} = \left.\frac{\partial^2 r_R(x_R)}{\partial x_R^2}\right|_{x_R=0} = 0$$

$$\begin{cases} \left.\dfrac{\partial r_i(x_i)}{\partial x_i}\right|_{x_i=l_i} = \left.\dfrac{\partial r_{i+1}(x_{i+1})}{\partial x_{i+1}}\right|_{x_{i+1}=0}, \\ \left.\dfrac{\partial^2 r_i(x_i)}{\partial x_i^2}\right|_{x_i=l_i} = \left.\dfrac{\partial^2 r_{i+1}(x_{i+1})}{\partial x_{i+1}^2}\right|_{x_{i+1}=0} \quad (i = 1, 2, \ldots, R-2), \end{cases}$$

$$\left.\frac{\partial r_{R-1}(x_{R-1})}{\partial x_{R-1}}\right|_{x_{R-1}=l_{R-1}} = -\left.\frac{\partial r_R(x_R)}{\partial x_R}\right|_{x_R=l_R},$$

$$\left.\frac{\partial^2 r_{R-1}(x_{R-1})}{\partial x_R^2 - 1}\right|_{x_{R-1}=l_{R-1}} = \left.\frac{\partial^2 r_R(x_R)}{\partial x_R^2}\right|_{x_R=l_R}.$$

Substituting the boundary conditions into equation (5), the mode shape of the continuous beam can be written as

$$\phi(x) = \begin{cases} A_1(\sin(\beta x) - \dfrac{\sin(\beta l_1)}{\sinh(\beta l_1)}\sinh(\beta x)), \quad 0 \leqslant x \leqslant l_1, \\ A_i\left(\sin\left(\beta\left(x - \sum_{j=1}^{i-1} l_j\right)\right) - \dfrac{\sin(\beta l_i)}{\sinh(\beta l_i)}\sinh\left(\beta\left(x - \sum_{j=1}^{i-1} l_j\right)\right)\right) + B_i\left(\cos\beta\left(\beta\left(x - \sum_{j=1}^{i-1} l_j\right)\right)\right. \\ \qquad \left. - \cosh\left(\beta\left(x - \sum_{j=1}^{i-1} l_j\right)\right) + \dfrac{\cosh(\beta l_i) - \cos(\beta l_i)}{\sinh(\beta l_i)}\sinh\left(\beta\left(x - \sum_{j=1}^{i-1} l_j\right)\right)\right), \\ \qquad \sum_{j=1}^{i-1} l_j \leqslant x \leqslant \sum_{j=1}^{i} l_j \quad (i = 2, 3, \ldots, R-1), \\ A_R(\sin(\beta(L - x)) - \dfrac{\sin(\beta l_R)}{\sinh(\beta l_R)}\sinh(\beta(L - x))), \quad L - l_R \leqslant x \leqslant L, \end{cases} \tag{6}$$

where parameters β, A_1, A_i, $B_i (i = 2, 3, \ldots, R-1)$, A_R are determined from equation (7) by solving the following set of equations [14]:

$$[F]\{A\} = 0, \tag{7}$$

where

$$A = \{A_1, A_2, B_2, \ldots, A_{R-1}, B_{R-1}, A_R\}.$$

The elements in matrix **F** are given by

$$f_{11} = \cos(\beta l_1) - \theta_1 \cosh(\beta l_1), \qquad f_{12} = \theta_2 - 1, \qquad f_{13} = -\phi_2,$$

$$f_{21} = \sin(\beta l_1), \qquad f_{23} = -1,$$

$$
\begin{aligned}
f_{2i-1,\,2(i-1)} &= \cos(\beta l_i) - \theta_i \cosh(\beta l_i),\\
f_{2i-1,\,2i-1} &= -\sin(\beta l_i) - \sinh(\beta l_i) + \phi_i \cosh(\beta l_i),\\
f_{2i-1,\,2i} &= \theta_{i+1} - 1,\\
f_{2i-1,\,2i+1} &= -\phi_{i+1},\\
f_{2i,\,2(i-1)} &= -\sin(\beta l_i) - \theta_i \sinh(\beta l_i),\\
f_{2i,\,2i-1} &= -\cos(\beta l_i) - \cosh(\beta l_i) + \phi_i \sinh(\beta l_i),\\
f_{2i,\,2i+1} &= 2 \quad (i = 2, 3, \ldots, R-2),\\
f_{2R-1,\,2(R-2)} &= -\cos(\beta l_{R-1}) + \theta_{R-1} \cosh(\beta l_{R-1}),\\
f_{2R-1,\,2R-1} &= \sin(\beta l_{R-1}) + \sinh(\beta l_{R-1}) - \phi_{R-1} \cosh(\beta l_{R-1}),\\
f_{2R-1,\,2(R-1)} &= \theta_R \cosh(\beta l_R) - \cos(\beta l_R),\\
f_{2(i-1),\,2(i-2)} &= \sin(\beta l_{R-1}) + \theta_{R-1} \sinh(\beta l_{R-1}),\\
f_{2(i-1),\,2i-1} &= \cos(\beta l_{R-1}) + \cosh(\beta l_{R-1}) - \phi_{R-1} \sinh(\beta l_{R-1}),\\
f_{2(i-1),\,2(i-1)} &= -2\sin(\beta l_R),
\end{aligned}
$$

where

$$
\theta_i = \frac{\sin(\beta l_i)}{\sinh(\beta l_i)}, \qquad \phi_i = \frac{\cosh(\beta l_i) - \cos(\beta l_i)}{\sinh(\beta l_i)} \quad (i = 1, 2, \ldots, R)
$$

and the other coefficients f_{ij} equal to zero.

2.3. GENERALIZED ORTHOGONAL FUNCTION EXPANSION

The strain in the beam at a point x and time t can be written as

$$
\varepsilon(x, t) = -h \frac{\partial^2 w(x, t)}{\partial x^2}, \tag{8}
$$

where h is the distance between the lower surface and the neutral plane of bending of the beam. Substituting equation (2) into equation (8) and assuming there are N modes in the responses, we have

$$
\varepsilon(x, t) = \boldsymbol{\varphi}\mathbf{Q}, \tag{9}
$$

where

$$
\boldsymbol{\varphi} = -\{h\phi_1''(x), h\phi_2''(x), \cdots, h\phi_N''(x)\}, \qquad \mathbf{Q} = \{q_1(t), q_2(t), \ldots, q_N(t)\}^{\mathrm{T}}.
$$

and $\phi_i''(x)$ is the second derivative of $\phi_i(x)$.

The strain can be approximated by a generalized orthogonal function $T(t)$ as

$$
\varepsilon(x, t) = \sum_{i=1}^{N_f} T_i(t) C_i(x) \tag{10}
$$

where $\{T_i(t), i = 1, 2, \ldots, N_f\}$ are the generalized orthogonal functions; $\{C_i(x), i = 1, 2, \ldots, N_f\}$ is the vector of coefficients in the expanded expression. The strains at the N_s measuring points can be expressed as

$$\boldsymbol{\varepsilon} = \mathbf{CT}, \tag{11}$$

where

$$\mathbf{T} = \{T_0(t), T_1(t), \ldots, T_{N_f}(t)\}^{\mathrm{T}},$$

$$\boldsymbol{\varepsilon} = \{\varepsilon(x_1, t), \varepsilon(x_2, t), \ldots, \varepsilon(x_{N_s}, t)\}^{\mathrm{T}},$$

$$\mathbf{C} = \begin{bmatrix} C_{10}(x_1) & C_{11}(x_1) & \cdots & C_{1N_f}(x_1) \\ C_{20}(x_2) & C_{21}(x_2) & \cdots & C_{2N_f}(x_2) \\ \vdots & \vdots & \vdots & \vdots \\ C_{N_s0}(x_{N_s}) & C_{N_s1}(x_{N_s}) & \cdots & C_{N_sN_f}(x_{N_s}) \end{bmatrix}$$

and $\{x_1, x_2, \ldots, x_{N_s}\}$ is the vector on the location of the strain measurements. By the least-squares method, the coefficient matrix can be obtained as

$$\mathbf{C} = \boldsymbol{\varepsilon}\mathbf{T}^{\mathrm{T}}(\mathbf{T}\mathbf{T}^{\mathrm{T}})^{-1}. \tag{12}$$

Substitute equation (9) into equation (11),

$$\mathbf{Q} = (\boldsymbol{\Phi}^{\mathrm{T}}\boldsymbol{\Phi})^{-1}\boldsymbol{\Phi}^{\mathrm{T}}\mathbf{CT}, \tag{13}$$

where

$$\boldsymbol{\Phi} = -\begin{bmatrix} h\phi_1''(x_1) & h\phi_2''(x_1) & \cdots & h\phi_N''(x_1) \\ h\phi_1''(x_2) & h\phi_2''(x_2) & \cdots & h\phi_N''(x_2) \\ \vdots & \vdots & \vdots & \vdots \\ h\phi_1''(x_{N_s}) & h\phi_2''(x_{N_s}) & \cdots & h\phi_N''(x_{N_s}) \end{bmatrix}$$

and it can be obtained from equation (6).

2.4. REGULARIZATION

The vector of generalized co-ordinates obtained from equation (13) can be substituted into equation (3), and rewritten it in a matrix form to become

$$\mathbf{I}\ddot{\mathbf{Q}} + \mathbf{C}_d\dot{\mathbf{Q}} + \mathbf{KQ} = \mathbf{BP}, \tag{14}$$

where

$$\mathbf{C}_d = \mathrm{diag}(2\xi_i\omega_i),$$

$$\mathbf{K} = \mathrm{diag}(\omega_i^2),$$

$$\mathbf{B} = \begin{bmatrix} \phi_1(\hat{x}_1(t))/M_1 & \phi_1(\hat{x}_2(t))/M_1 & \cdots & \phi_1(\hat{x}_{N_p}(t))/M_1 \\ \phi_2(\hat{x}_1(t))/M_2 & \phi_2(\hat{x}_2(t))/M_2 & \cdots & \phi_2(\hat{x}_{N_p}(t))/M_2 \\ \vdots & \vdots & \vdots & \vdots \\ \phi_N(\hat{x}_1(t))/M_N & \phi_N(\hat{x}_2(t))/M_N & \cdots & \phi_N(\hat{x}_{N_p}(t))/M_N \end{bmatrix}.$$

The required $\ddot{\mathbf{Q}}$ and $\dot{\mathbf{Q}}$ can be obtained by directly differentiating equation (13) to have

$$\ddot{\mathbf{Q}} = (\mathbf{\Phi}^{\mathrm{T}}\mathbf{\Phi})^{-1}\mathbf{\Phi}^{\mathrm{T}}\mathbf{C}\ddot{\mathbf{T}},$$

$$\dot{\mathbf{Q}} = (\mathbf{\Phi}^{\mathrm{T}}\mathbf{\Phi})^{-1}\mathbf{\Phi}^{\mathrm{T}}\mathbf{C}\dot{\mathbf{T}}.$$

The moving forces obtained from equation (14) using a straightforward least-squares solution would be unbound. Let the left-hand side of equation (14) be represented by $\mathbf{U}$. A regularization technique can be used to solve the ill-posed problem in the form of minimizing the function

$$\mathbf{J}(\mathbf{P}, \lambda) = \|\mathbf{BP} - \mathbf{U}\|^2 + \lambda\|\mathbf{P}\|^2, \tag{15}$$

where λ is the non-negative regularization parameter.

2.5. OPTIMAL REGULARIZATION PARAMETER

The success of solving equation (15) lies in how to determine the regularization parameter λ. Two methods are used in this paper. If the true forces are known, the parameter can be determined by minimizing the error between the true forces and the predicting values as

$$S = \|\hat{\mathbf{P}} - \mathbf{P}\|. \tag{16}$$

In the real case when the true forces are not known, the method of generalized cross-validation (GCV) is used to determine the optimal regularization parameter. The GCV function to be minimized in this work is defined by [5]

$$\mathbf{g}(\lambda) = \frac{\|\mathbf{B}\hat{\mathbf{P}} - \mathbf{U}\|_2^2}{\{\mathrm{trace}[\mathbf{I} - \mathbf{B}((\mathbf{B}^{\mathrm{T}}\mathbf{B} + \lambda\mathbf{I})^{-1}\mathbf{B}^{\mathrm{T}})^{-1}]\}^2}, \tag{17}$$

where $\hat{\mathbf{P}}$ is the vector of estimated forces.

3. NUMERICAL EXAMPLES

3.1. MOVING FORCES

The proposed method is illustrated in the following simulation studies. The effect of discarding some of the information contained in the measured responses on the identification errors is studied. This aspect has not been studied in previous works reported by the authors or by other researchers.

3.1.1. *Single-span beam*

A single span simply supported beam is studied with two varying forces moving on top at a constant spacing of 4·27 m.

$$\begin{aligned} f_1(t) &= 9{\cdot}9152 \times 10^4[1 + 0{\cdot}1\sin(10\pi t) + 0{\cdot}05\sin(40\pi t)] \quad \mathrm{N}, \\ f_2(t) &= 9{\cdot}9152 \times 10^4[1 - 0{\cdot}1\sin(10\pi t) + 0{\cdot}05\sin(50\pi t)] \quad \mathrm{N}. \end{aligned} \tag{18}$$

The parameters of the beam are as follows: $EI = 2{\cdot}5 \times 10^{10}\ \mathrm{N\,m^2}$, $\rho A = 5000\ \mathrm{kg/m}$, $L = 30\ \mathrm{m}$, $h = 1\ \mathrm{m}$. The first eight natural frequencies of the beam are 3·9, 15·61, 35·13,

TABLE 1

Identified errors for single-span beam

	Noise level					
	1%		5%		10%	
Number of mode shapes	First force	Second force	First force	Second force	First force	Second force
2	31·51	31·53	45·11	45·05	174·27	112·50
3	11·56	12·00	13·04	13·24	16·31	16·08
4	6·78	6·18	7·05	6·95	8·47	8·69
5	5·16	3·62	5·07	3·89	5·46	4·80
6	3·90	3·10	4·02	3·28	4·14	3·66
7	3·43	2·99	3·45	3·13	3·66	3·44
8	3·15	2·86	3·19	3·01	3·42	3·29
9	9·52	8·96	9·48	8·94	9·48	8·94
10	18·02	17·30	18·51	17·99	18·42	17·88

62·48, 97·58, 140·51, 191·25 and 249·8 Hz, and they are used in the computation of the analytical mode shapes from equation (6). The forces are moving at a speed of 30 m/s. Random noise is added to the calculated strains to simulate the polluted measurement and 1, 5 and 10% noise levels are studied with

$$\varepsilon = \varepsilon_{calculated} + Ep \cdot N_{iose} \cdot \mathrm{var}(\varepsilon_{calculated}) \tag{19}$$

where ε is the vector of strains; Ep is the noise level; N_{iose} is a standard normal distribution vector with zero mean and unit standard deviation; $\varepsilon_{calculated}$ is the vector of calculated strains; $\mathrm{var}(\varepsilon_{calculated})$ is the standard deviation of $\varepsilon_{calculated}$. The errors in the identified forces are calculated as

$$Error = \frac{\|\hat{\mathbf{P}} - \mathbf{P}_{True}\|}{\|\mathbf{P}_{True}\|} \times 100\%. \tag{20}$$

Table 1 shows the errors of identification from the use of different number of mode shapes in the identification. The time step is 0·001 s in the calculation. The strain consists of responses from the first eight mode shapes polluted with 5% noise level. Ten measuring points are available in the identification and they are evenly distributed along the beam length. The different combinations of number of mode shapes used in the identification and the number of measuring points are studied. Figure 3 shows the identified results using three and six mode shapes. The following observations are obtained.

(1) Results in Table 1 show that the errors in the identified forces are insensitive to the noise level in the responses. This is because orthogonal functions have been used to approximate the strains in the identification, and this approximation suppresses the errors due to high-frequency measurement noise.
(2) When the number of mode shapes used in the identification is the same as the number of mode shapes in the responses, i.e. eight mode shapes, the identified errors are the smallest. The errors in identification become large when the number of mode shapes used in the identification is either larger or smaller than the number of mode shapes in the responses. This indicates that the pairing of the number of mode shapes in both

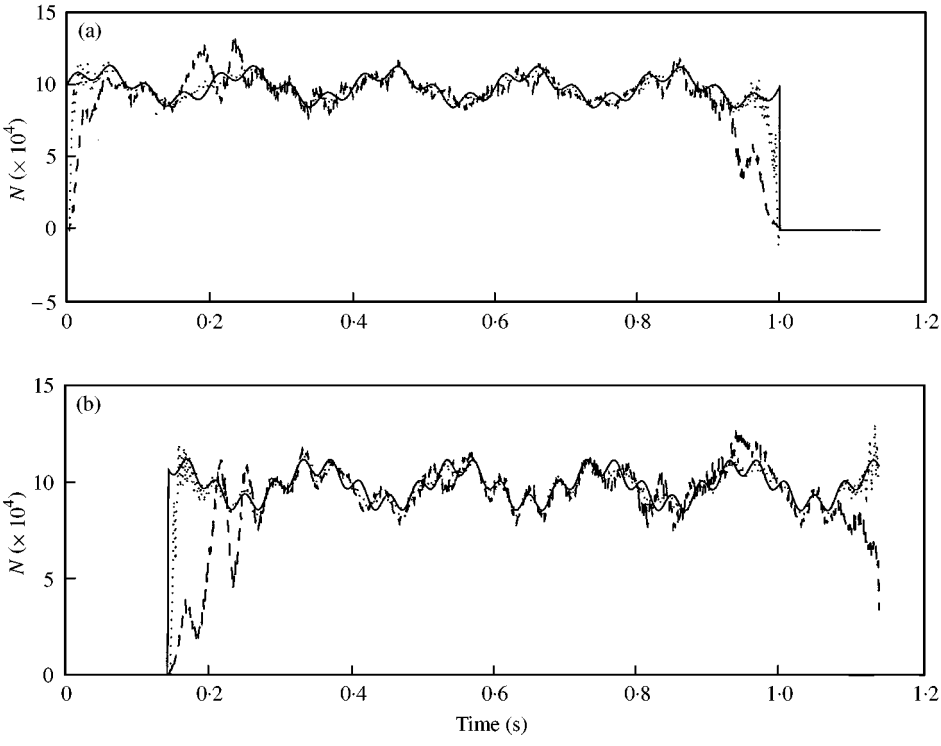

Figure 3. The identified results with different number of mode shapes: ——, (a) The first axle force, (b) The second axle force. true loads; – – – –, identified results with three modes; ·····, identified results with six modes.

the responses and the identified forces has a large effect on the errors in the identification. The correct pairing can be determined from an inspection of the frequency content in the measured responses.

(3) Figure 3 shows that there are large discrepancies in the identified forces near the beginning and the end of the moving forces when only three modes are used in the identification. These discrepancies are much less when six modes are used. This is because of the sudden appearance and disappearance of the forces at these points which can be represented by an equivalent impulse force. These impulsive forces excite the beam with a broadband vibration that covers a large number of modal frequencies. Therefore, more mode shapes should be used in the identification to take advantage of the information of the forces at higher modal frequencies in the responses at the beginning and the end of the time histories.

3.1.2. *Two-span-continuous beam*

Table 2 shows the errors in the identified moving forces on a two-span continuous beam with different number of mode shapes and number of measuring points. The parameters of the beam are the same as for the single-span beam except each span measures 30 m long. The first eight natural frequencies of the beam are 3·9, 6·1, 15·61, 19·75, 35·12, 41·22, 62·43 and 70·48 Hz. Figure 4 shows the identified forces from using strains polluted with 5% noise level at six measuring points. Inspection of the results in Table 2 and Figure 4 gives the following observations:

TABLE 2

Identified errors for two-span beam

No. of mode shapes in responses N_1	No. of mode shapes in identification N_2	No. of measuring points N_s	Noise level					
			1%		5%		10%	
			First force	Second force	First force	Second force	First force	Second force
10	10	14	7·85	9·07	18·48	19·44	27·64	28·99
10	10	10	7·78	8·98	16·67	17·98	26·28	27·42
10	9	10	8·90	10·61	15·95	17·23	24·24	25·12
10	8	10	11·54	13·71	23·05	24·12	31·37	32·59
10	7	10	13·81	16·19	17·02	19·01	21·99	23·70
10	6	10	17·05	19·55	20·76	22·99	26·61	28·54
6	6	6	15·99	18·15	20·15	21·91	26·26	27·78
6	6	8	16·06	18·21	20·93	22·69	27·74	29·24
6	6	10	15·98	18·15	19·98	21·77	26·11	27·69
6	6	12	15·90	18·08	18·90	20·73	24·02	25·65
6	6	14	15·85	18·04	18·19	20·06	22·47	24·14

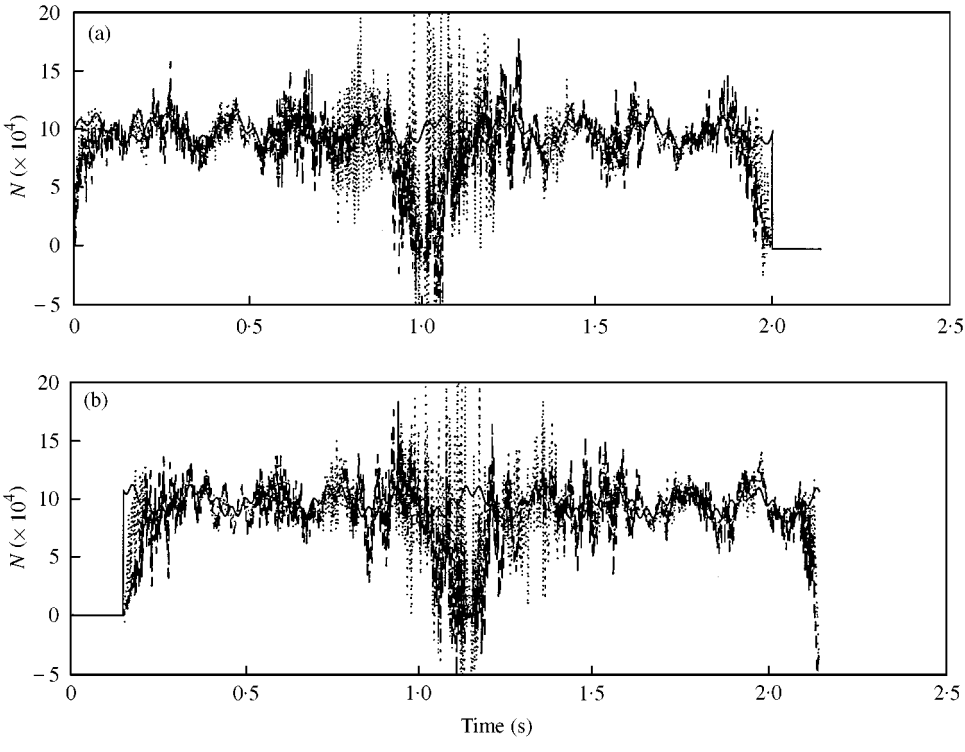

Figure 4. The identified results with different number of mode shapes: (a) The first axle force. (b) The second axle force. ——, true loads; – – – –, identified results with three modes; ·····, identified results with six modes.

(1) Results in Table 2 show that the errors increase as the noise level in the response increases. The errors are more than twice of that under similar conditions for the single-span beam. Therefore, moving load identification in a multi-span beam would be less accurate than that in a single-span beam.
(2) When the number of mode shapes used in the identification equals to that in the responses as shown in the first two rows and the lower part of Table 2, the errors in the identified forces vary only slightly with more measuring points. The number of the measuring points is best selected to be equal to the number of mode shapes.
(3) Results from the upper part of Table 2 also show that the errors would be smallest when the number of mode shapes in the identification is the same as that in the responses. This confirms the observation made in the case of the single-span beam.
(4) The identified forces in Figure 4 have large fluctuations close to zero at the point of the intermediate support at 1·0 s. This is again due to the presence of the equivalent impulsive force with the sudden appearance or disappearance of the forces at this point.

3.2. BRIDGE–VEHICLE INTERACTION FORCES

Figure 5 shows a vehicle system with 4-d.o.f.s with damping included [15]. The axle spacing is 4·27 m. The vehicle is simulated as moving on top of an unequal three-span uniform bridge deck at a velocity of 30 m/s. The parameters and natural frequencies of the bridge and vehicle are shown in Table 3. The bridge responses and the interaction forces are

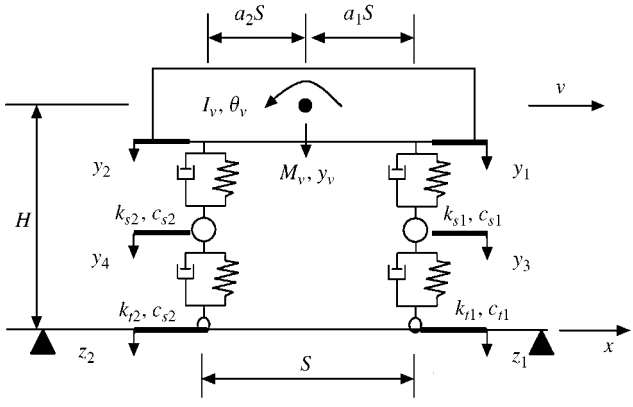

Figure 5. A bridge–vehicle system.

TABLE 3

Parameters of the three-span bridge and the 4-d.o.f.s vehicle

Parameters of the three-span bridge	Parameters of the vehicle (Mulcahy, 1983)
$L_1 = L_3 = 30$ m, $L_2 = 50$ m $\rho = 5{\cdot}0 \times 10^3$ kg/m $EI = 2{\cdot}5 \times 10^{10}$ N m^2 $I = 1{\cdot}8 \times 10^5$ kg/m^2 $\xi = 2\%$ Natural Frequencies (Hz) 2·07, 4·44, 5·21, 7·69, 13·82, 17·24, 18·82, 25·63, 35·12, 38·18, 41·84, 54·23	$M_v = 17\,735$ kg, $m_1 = 1500$ kg, $m_2 = 1000$ kg $I_v = 1{\cdot}47 \times 10^5$ kg m^2 $k_{s1} = 2{\cdot}47 \times 10^6$ N m^{-1}, $k_{s2} = 4{\cdot}23 \times 10^6$ N/m $k_{t1} = 3{\cdot}74 \times 10^6$ N m^{-1}, $k_{t2} = 4{\cdot}60 \times 10^6$ N/m $c_{s1} = 30\,000$ N s/m; $c_{s2} = 40\,000$ N s/m $c_{t1} = 3900$ N s/m; $c_{t2} = 4300$ N s/m $a_1 = 0{\cdot}519$; $a_2 = 0{\cdot}481$; $H = 1{\cdot}80$

calculated by the method proposed by Henchi *et al.* [16]. The time step in the calculation is 0·005 s. The road surface roughness of the bridge is not included in the simulation. The measuring points are evenly distributed along each span. The identified axle loads from the following two cases using different number of modes and measuring points are shown in Figure 6. The number of mode shapes in the identification is taken to be equal to that in the measured responses.

Case 1: The first six modes and eight measuring points are used in the identification. There are two measuring points spaced at one-third span on the first span and the third span, and four measuring points spaced at one-fifth span on the second span.

Case 2: The first 12 modes and 14 measuring points are used in the identification. There are four measuring points spaced at one-fifth span on the first span and the third span, and six measuring points spaced at one-seventh span on the second span.

1% noise is included in the responses. Figure 6 shows that the identified results are close to the calculated interaction forces except near the supports, and Case (2) gives more accurate results than Case (1) particularly at locations close to the supports. Therefore, the proposed method is also effective for identifying the bridge–vehicle interaction forces.

Comparison with previous published results shows that the identified forces at the supports are discontinuous in this work while those from Zhu and Law [11] are continuous. This is because the large stiffness support assumption in the latter case enables

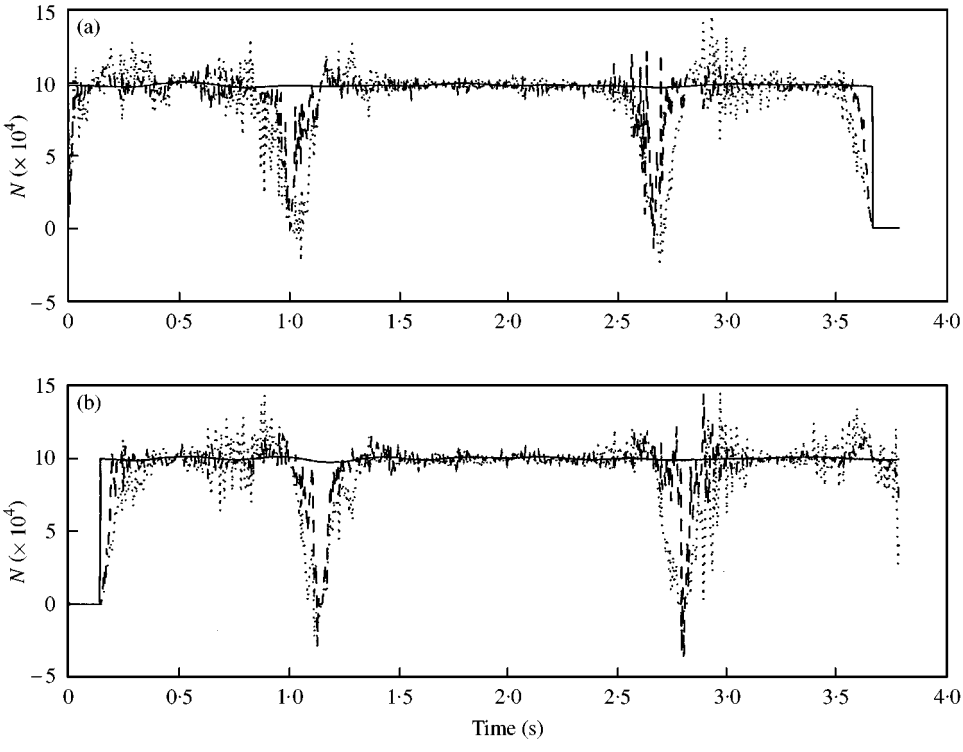

Figure 6. The identified results with different modes and measuring points: (a) The first axle force. (b) The second axle force. ——, calculated interaction forces; ·····, identified results with six modes and eight measuring points; – – – –, identified with 12 modes and 14 points.

small continuous responses of the beam when the force is over the support, while those of the beam in the present case equal to zero when the force is over the support.

4. EXPERIMENT

4.1. EXPERIMENTAL SETUP AND MEASUREMENTS

The experimental setup is shown diagrammatically in Figure 7. The main beam, 3678 mm long with a 100 mm × 25 mm uniform cross-section, is simply supported. There is a leading beam for accelerating the vehicle and a tailing beam to accept the vehicle when it comes out of the main beam. A U-shaped aluminum section is glued to the upper surface of the beams as a direction guide for the car. The model car is pulled along the guide by a string wound around the drive wheel of an electric motor. Thirteen photoelectric sensors are mounted on the beams to measure and monitor the moving speed of the car. Six strain gauges are evenly located on the beam to measure the bending moment responses of the beam. A TEAC 11-channels magnetic tape recorder and an 8-channel dynamic testing and analysis system are used for data collection and analysis in the experiment. The sampling frequency is 2000 Hz. The recorded length of each test lasts for 6 s. The model car has two axles at a spacing of 0·557 m and it runs on four steel wheels with rubber band on the outside. The mass of the whole car is 16·6 kg with 9·8 and 6·8 kg as the first and second static axle forces respectively.

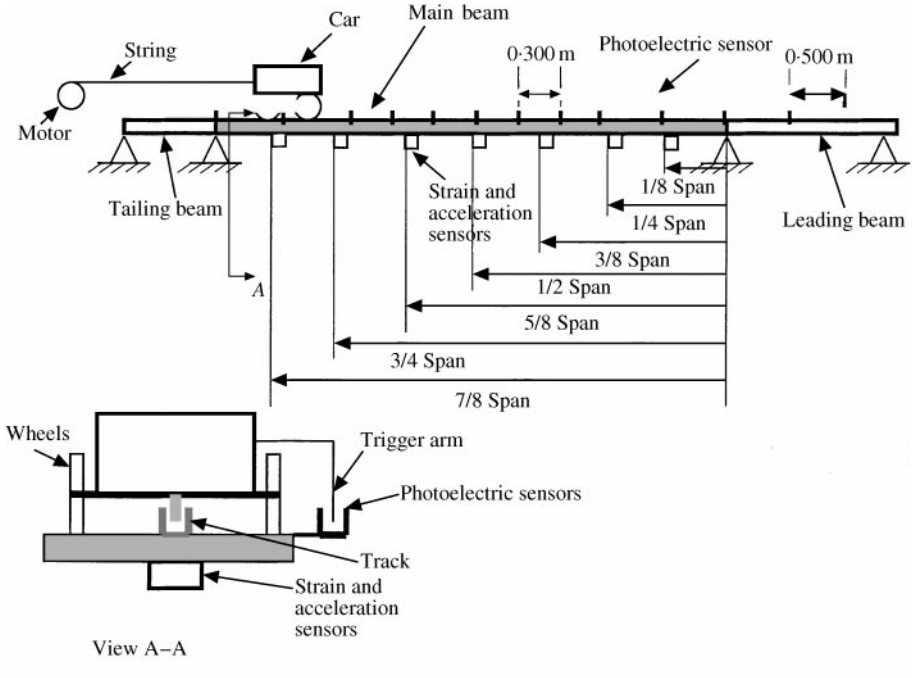

Figure 7. Diagrammatic illustration of the experimental setup.

TABLE 4

The correlation coefficients between measured and reconstructed responses at 5/8*L*

Case	Number of mode shapes	Measuring locations	Correlation coefficient
A	3	1/4*L*, 1/2*L*, 3/4*L*,	0·9809
B	4	1/8*L*, 1/4*L*, 1/2*L*, 3/4*L*	0·9470
C	5	1/8*L*, 1/4*L*, 1/2*L*, 3/4*L*, 7/8*L*	0·9752
D	3	1/8*L*, 1/4*L*, 3/8*L*, 1/2*L*, 3/4*L*, 7/8*L*	0·9853
E	4	1/8*L*, 1/4*L*, 3/8*L*, 1/2*L*, 3/4*L*, 7/8*L*	0·9837
F	5	1/8*L*, 1/4*L*, 3/8*L*, 1/2*L*, 3/4*L*, 7/8*L*	0·9822
G	6	1/8*L*, 1/4*L*, 3/8*L*, 1/2*L*, 3/4*L*, 7/8*L*	0·9716

4.2. FORCE IDENTIFICATION

Strains at 1/8*L*, 1/4*L*, 3/8*L*, 1/2*L*, 3/4*L*, 7/8*L* are used in the identification. Table 4 shows the correlation coefficients between the measured and the reconstructed strains at 5/8*L* from the identified forces with different number of mode shapes in the identification. The number of measuring points and the number of mode shapes are shown in Table 4. Figure 8 shows the identified forces from Cases (A) and (G) of the study using three and six sensors respectively. The combined force is also presented in Figure 8(c). The following observations are made.

(1) Table 4 shows that the correlation coefficients are all larger than 0·9 for different combinations of modes and measuring points. It shows that the proposed method is effective to identify the moving forces in practice.

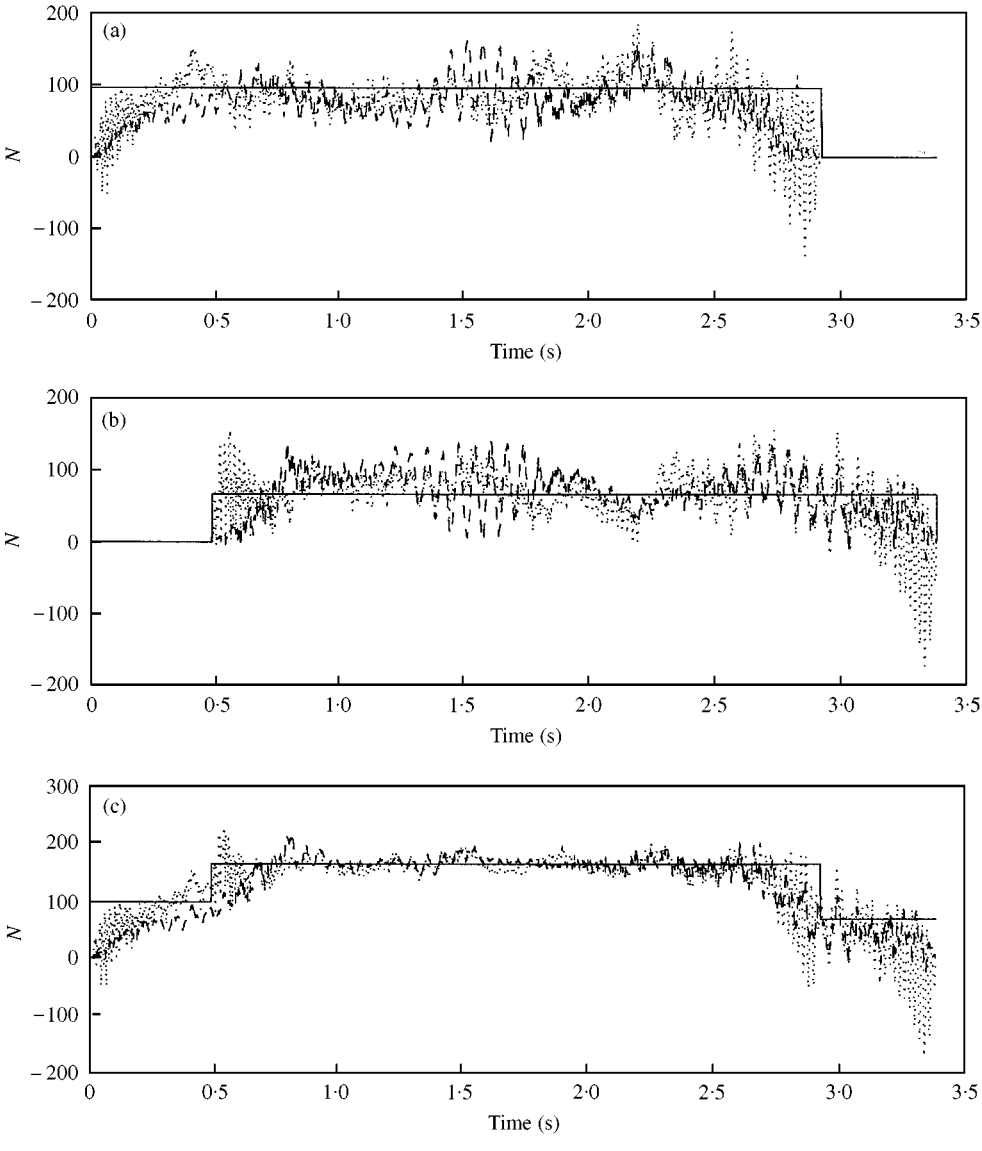

Figure 8. Identified results from using different modes. (a) The first axle force. (b) The second axle force. (c) The resultant force. ——, static load; – – – –, with three modes (Case A); · · · · ·, with six modes (Case G).

(2) There is a low-frequency component in the identified individual forces in Figure 8. This is the pitching motion of the moving car.
(3) The identified forces from using six modes are closer to the static forces at the beginning and the end of the time histories than that obtained from using three modes. This gives experimental evidence of the fact that more mode shapes in the computation should be used to identify the moving forces near these locations.

5. CONCLUSIONS

This paper presents several improvements on the accuracy of moving force identification. An improved formulation on the analytical vibration mode shapes of a continuous beam on

rigid supports is presented, and these mode shapes are used instead of the assumed mode shapes in the inverse problem of moving force identification. A generalized orthogonal function approach is proposed to obtain the modal velocity and acceleration from measured strain response. This reduces the error due to measurement noise. The moving forces are identified with bounds in the errors using regularization method in the solution. Observations on the computation simulations and experimental test results provide evidence to the following conclusions.

(1) The proposed moving force identification method is effective for identifying the moving loads from measured strains in a multi-span bridge in time domain.
(2) The proposed method can be used to identify the bridge–vehicle interaction forces from measured strains in a continuous beam, and acceptable results can be obtained.
(3) More mode shapes should be used to identify the moving forces at locations close to the supports.
(4) When the number of mode shapes in the identification is the same as that in the measured responses, the errors of identification will be the smallest.

ACKNOWLEDGMENTS

The work described in this paper was supported by a grant from the Hong Kong Polytechnic University Research Funding Project No. V653. This work was carried out under the supervision of the second author.

REFERENCES

1. H. Lee and Y.-S. Park 1995 *Mechanical Systems and Signal Processing* **9**, 615–633. Error analysis of indirect force determination and a regularization method to reduce force determination error.
2. H. R. Busby and D. M. Trujillo 1987 *Computers and Structures* **25**, 109–117. Solution of an inverse dynamics problem using an eigenvalue reduction technique.
3. H. R. Busby and D. M. Trujillo 1997 *Computers and Structures* **63,** 243–248. Optimal regularization of an inverse dynamics problem.
4. P. C. Hansen 1992 *SIAM Review* **34**, 561–580. Analysis of discrete ill-posed problems by means of the L-Curve.
5. G. H. Golub, M. Heath and G. Wahba 1979 *Technometrics* **21**, 215–223. Generalized cross-validation as a method for choosing a good ridge parameter.
6. D. C. Kammer 1998 *American Society of Mechanical Engineers Journal of Vibration and Acoustics* **120**, 868–874. Input force reconstruction using a time domain technique.
7. C. O'Connor and T. H. T. Chan 1988 *American Society of Civil Engineers Journal of Structural Engineering* **114**, 1703–1723. Dynamic wheel loads from bridge strains.
8. T. H. T. Chan, S. S. Law, T. H. Yung and X. R. Yuan 1999 *Journal of Sound and Vibration* **219**, 503–524. An interpretive method for moving forces identification.
9. S. S. Law, T. H. T. Chan and Q. H. Zeng 1997 *Journal of Sound and Vibration* **201**, 1–22. Moving force identification: A time domain method.
10. S. S. Law, T. H. T. Chan and Q. H. Zeng 1999 *American Society of Mechanical Engineers Journal of Dynamic Systems, Measurement, and Control* **121**, 394–401. Moving force identification—a frequency and time domains analysis.
11. X. Q. Zhu and S. S. Law 1999 *Journal of Sound and Vibration* **228**, 377–396. Moving forces identification on a multi-span continuous bridge.
12. Y. H. Lin 1995 *Journal of Sound and Vibration* **180**, 809–812. Comments on "Dynamic response of a beam with intermediate point constraints subject to a moving load".
13. T. Hayashikawa and N. Watanabe 1981 *American Society of Civil Engineers Journal of the Engineering Mechanics Division* **107**, 229–246. Dynamic behavior of continuous beams with moving loads.

14. D. J. GORMAN 1975 *Free Vibration Analysis of Beams and Shafts*. New York: John Wiley & Sons.
15. N. L. MULCAHY 1983 *Earthquake Engineering and Structural Dynamics* **20**, 649–665. Bridge response with tractor-trailer vehicle loading.
16. K. HENCHI, M. FAFARD, M. TALBOT and G. DHATT 1998 *Journal of Sound and Vibration* **212**, 663–683. An efficient algorithm for dynamic analysis of bridges under moving vehicles using a coupled modal and physical components approach.

APPENDIX A: NOMENCLATURE

The following symbols are used in this paper.

h	distance between the lower surface to the neutral plane of bending
$\mathbf{C}_d$	damping coefficient of the beam
$w(x, t)$	transverse displacement of the beam
$\varepsilon(x, t)$	strains in the beam
ρ	mass density of material
$P_i(t)$	the ith moving load
$\hat{x}_i(t)$	location of the ith moving load
N_p	number of moving loads
N_f	number of terms in the orthogonal function
N_s	number of measuring points
N	number of mode shapes used
$q_i(t)$	ith modal coordinate
ω_i	ith circular frequency in radians per second
$\mathbf{M}$, $\mathbf{K}$, $\mathbf{C}$	mass, stiffness, and damping matrices
$\hat{\mathbf{P}}$	vector of estimated forces
$\mathbf{Q}$	vector of modal co-ordinates
$\varphi(x)$	mode shape of the continuous beam
$\delta(x)$	Dirac function
λ	regularization parameter
β, r_1	eigenvalue and eigenfunction of the continuous beam
k_{t1}, k_{t2}	stiffness of tyres
c_{t1}, c_{t2}	damping in tyres
k_{s1}, k_{s2}	stiffness of axle assemblies
c_{s1}, c_{s2}	damping of axle assemblies
m_v	mass of car body
I_v	torsional moment of inertia of car body